Title: Magnetically actuated dexterous tools for minimally invasive operation inside the brain

Authors:
Changyan He[1,2†], Robert Nguyen[2], Haley Mayer[1,2,3], Lingbo Cheng[4], Paul Kang[2,5], D. Anastasia Aubeeluck[1], Grace ThiongO[2], Erik Fredin[1], James Drake[2], Thomas Looi[2], Eric Diller[1,3,5]*

Affiliations:
[1]Department of Mechanical and Industrial Engineering, University of Toronto; Toronto, Canada.
[2]PCIGITI Center, The Hospital for Sick Children; Toronto, Canada.
[3]Robotics Institute, University of Toronto; Toronto, Canada.
[4]School of Engineering, University of Newcastle; Newcastle, Australia
[5]Institute of Biomedical Engineering, University of Toronto; Toronto, Canada.
[†]Present address: School of Engineering, University of Newcastle; Newcastle, Australia
*Corresponding author. Email: ediller@mie.utoronto.ca.

Abstract: Operating in the brain for deep-seated tumors or surgical targets for epilepsy is technically demanding and normally requires a large craniotomy with its attendant risk and morbidity. Neuroendoscopic surgery has the potential to reduce risk and morbidity by permitting surgical access through a small incision with burr hole and a narrow corridor through the brain. However, current endoscopic neurosurgical tools are straight and rigid and lack dexterity, hindering their adoption for neuroendoscopic procedures. We propose a class of robotic neurosurgical tools that have magnetically actuated wristed end effectors small enough to fit through a neuroendoscope working channel. The tools were less than 3.2 millimeters in overall diameter and contained embedded permanent magnets that allowed wireless actuation with magnetic fields. Three magnetic tools are presented: a two–degrees-of-freedom (DoFs) wristed gripper, a one-DoF pivoting scalpel, and a one-DoF twisted string–actuated forceps. This work evaluated the feasibility of these tools for completing minimally invasive neurosurgical resection and cutting tasks. Experimental tests on a silicone brain phantom showed that the tools could reach the ventricle area for simulated tumor removal and access a section of the corpus callosotomy for a simulated tissue-severing procedure in epilepsy treatment. Integration of the magnetic end effectors with a concentric tube robot as a hybrid steerable surgical robotic system enabled in vivo experiments on piglets. These experiments show that wireless magnetic tools could perform essential neurosurgical tasks, including gripping, cutting, and biopsy on living brain tissue, suggesting their potential for clinical applications.

One-Sentence Summary: We presented a class of endoscopic magnetic tools with dexterous wrists for minimally invasive neurosurgery.

INTRODUCTION

Neurological disorders pose a substantial burden on worldwide health, and severely affect patients' quality of life. Many of these disorders cannot be treated with medication – epilepsy for example represents one fourth of this neurological burden, and is frequently refractory to medication in up to 40% of patients (*1-3*). For these patients, surgery is an efficacious and cost effective treatment. Currently neurosurgeries are most commonly performed via an open approach, through large skin incisions in which the surgeon typically needs to remove a large portion of the patient's skull to expose the brain and create an operating corridor to access the diseased area by dissecting through healthy brain. Such invasive operations carry substantial risk to patients who also experience major morbidity, and prolonged hospital stays.

Endoscopic neurosurgery (*4*) is one approach aimed at reducing surgical morbidity and improving surgical outcomes in comparison with open surgical approaches. In such an endoscopic operation, a small burr hole is made through the skull, allowing for placement of an endoscope into the brain through a small incision in the brain. The surgeon inserts long thin surgical tools into the brain through the endoscope working channel. The incision on the skull and brain from an endoscopic approach is notably reduced as compared to that with open surgery; however, the surgeon's manipulation dexterity is severely reduced because the surgical tool is constrained by the narrow channel of the endoscope trocar. The surgeon can only move the endoscopic tool through advancement or retraction with limited pitching or yawing motion. This limited manipulation dexterity means that an endoscopic neurosurgery approach is rarely used clinically, and only for simple tasks such as biopsy. In conventional open neurosurgery tasks, the surgeon largely relies on their own dexterous wrist to pivot the tools and tilt the tooltip at a wide angle to access hard-to-reach areas such as removing a tumor inside the third ventricle. Such a "wristed" tool motion would be required for the surgeon to perform complex procedures in a minimally invasive approach.

In contrast to neurosurgery, abdominal surgery has been practiced with a laporascopic approach in general surgery, urology and gynecology for decades thanks to the availability of dexterous wristed laparoscopic robotic tools. The well known da Vinci surgical system (Intuitive Surgical), best exemplified by its use in radical prostatectomy where more than 50% of US cases are now performed robotically (*5*), enables surgeons to mimic natural hand motion with its 7-degree-of-freedom (DoF) instrument wrist. Such high-DoF robot motion mimics the surgeon's hand at the robot tip in a natural way, facilitating manipulation.

Despite this potential, a robotic approach to neuroendoscopy has yet to be clinically realized because of the requirement for the size of neuroendoscopy tools to be substantially smaller in diameter compared to general surgery laparoscopic tools (the da Vinci robotic EndoWrist instrument is 8 mm in diameter). The small tool diameter creates challenges in scaling down wristed instruments because of difficulties in fabrication, assembly, and friction in the cable driven mechanisms. Pulleys smaller than several millimeters in width to articulate the instrument tips are weak at this scale and prone to friction, stretch, and fracture. Progress in developing smaller scale wristed robotic end effectors have recently been made by MMI (FL, USA) (*6*) and Sony Group Corporation (Sony, Japan) (*7*), primarily for use in microvascular anastomoses. These robotic tools, similar to that of the da Vinci surgical system, use cable driven approach to deliver the

mechanical actuation to the end effector. However, a straight and rigid tool shaft is required for such a robot to accommodate the transmission cables to facilitate low friction transmissions, which makes the tools incapable of following curved paths inside complex anatomy with minimal invasiveness, for example the brain.

As a solution to this miniaturization challenge, slender robots such as concentric tube robots (CTRs) (*8-12*) and cable driven continuum robots (*13*, *14*) have been explored for potential use in endoscopic neurosurgery. Although such robots are steerable and can perform snake-like motions, they cannot perform end effector articulation similar to the human wrist with tight bends up to 90 degrees. More importantly, both CTRs and continuum robots have difficulties in adding a distal end effector (e.g., forceps) because they deliver power mechanically from base to tip along the long narrow channels. Curvature of the CTR or the continuum robot can increase the friction even more between the cable and the channel, causing instability of the robot (*15*)– a problem that worsens when the robot extends into tightly curved shapes. Adding a wireless end effector by leveraging magnetic fields (*16*) or other field sources (*17*) for actuation would potentially address this problem for CTRs and continuum robots. However, such magnetic end effectors have not been previously investigated. Some earlier research explored articulated robotic arms for neurosurgery such as NeuroArm (*18*), NeuroMate (*19*), and ROSA One Brain (*20*), but those works aimed at target localization for stereotactic procedures, and none of them offer the same "wrist like" motions at their tooltips.

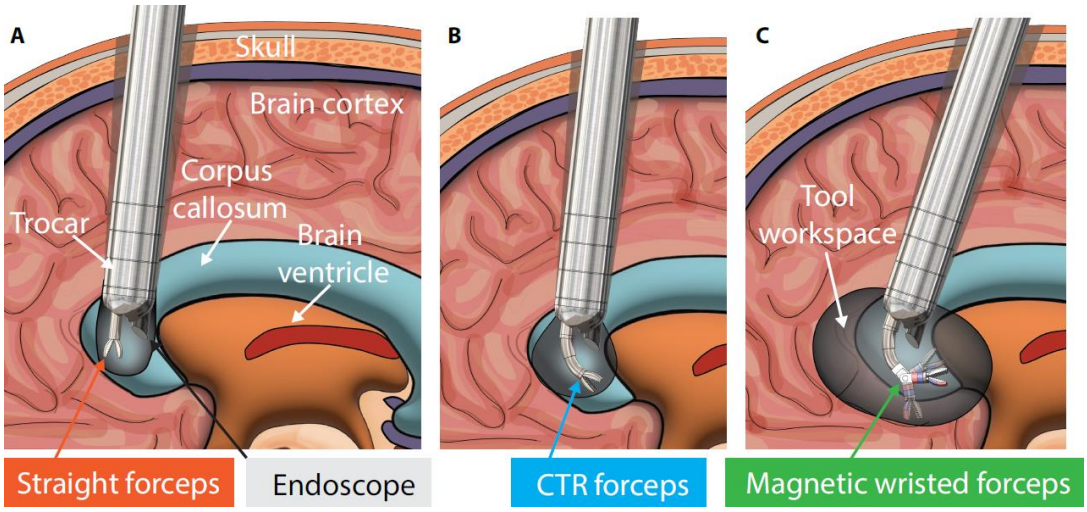

Figure 1. Endoscopic neurosurgery. In endoscopic procedures, the surgeon advances an endoscope trocar through the skull and brain tissue to approach the designated site. **A.** In most conventional endoscopic approaches, only a single rigid tool can be inserted through the trocar. **B.** Steerable tools such as CTR can provide enhanced reachability but cannot provide wristed motion. **C.** The magnetic tools with a field driven wrist enable a surgeon to control the tooltip with wristed motions similar to a dexterous wrist. The shaded region represents the reachable workspace for each tool type.

In this work, we avoid the challenges of mechanical cable and pulley driven mechanisms for neurosurgery through the use of magnetically actuated wristed mechanisms. These robotic end effectors, containing small magnets at their joints, are directly actuated by an external magnetic field and can perform dexterous multi-DoF articulation motions at their tips, as shown in Fig. 1. The wireless actuation approach avoids mechanism friction and therefore can facilitate the design of wristed robots at a small scale.

Magnetically actuated micro-robots have demonstrated substantial advantages in applications where a physical presence is required inside remote or enclosed micro-scale environments. However, most magnetic micro- and milli- robots are untethered devices for various delivery tasks (*21*, *22*) such as capsule endoscope (*23*-*25*), drug delivery (*26*, *27*), sample collection (*28*, *29*), cancer therapy (*30*), or soft catheter robots for endovascular catheterization (*31*-*35*). The effectiveness and dexterity of magnetically-driven surgical tools for tissue manipulations with millimeter-scale or smaller dimensions have yet to be investigated. Our previous works have investigated the feasibility of employing magnetic fields for powering surgical tools and proposed several prototypes for magnetic tools including wristed grippers (*36*, *37*), scissors (*38*), and miniaturized transmissions (*39*). In this work, we improve the magnetic tools' performance by considering clinical requirements in the design and further develop a complete clinically ready magnetic surgical tool system.

For use in endoscopic neurosurgery, magnetically driven end effectors need to meet the following requirements:

First, the robots should generate **sufficient operation forces** to manipulate brain tissue. Marcus et al. (*40*) reported that the forces necessary to manipulate brain tissue were relatively low; for example, the force needed to make an incision on most parts of the brain including the corpus callosum, the area that needs to be typically disconnected to treat epilepsy, is as low as 10 mN. Considering the procedures are generally more complex than simply incising and greater forces would be required, the value of 10 mN should be set as a lower limit for the magnetic robots' force output, with values of over 100 mN likely being required for resection and tissue cutting (*41*).

Additionally, the robots must be **small enough** to fit through the working channel of a neuro-endoscope trocar. Based upon currently utilized neuroendoscopic systems the overall diameter of a trocar can be up to 10 mm. Typically a trocar needs to provide corridors for an endoscope that is 2-3 mm in diameter and a working tool that should be smaller than 4-5 mm in diameter given the trocar's dimension limit. Taking this into account, the magnetic robots should be smaller than 4 mm in diameter.

Modularization is another essential design consideration. The magnetic robots with different end effectors should be interchangeable to conduct different tasks, for example, grasping with a gripper and cutting with scissors, which requires that the magnetic robots be modular in design and have a versatile interface.

Finally, the surgical workspace should **remain unobstructed** to provide surgeons with clear access to the patient. During a procedure, the surgeons should have an open workspace around the patient's head in case of the requirement for urgent access, which requires that the magnetic actuation system for the robots only occupy space under the operating table.

Taking these requirements into consideration, we designed a two-DoF magnetic robotic gripper for neurosurgical operations and developed a complete robotic system for magnetic actuation and robotic positioning that comprised an electromagnetic system and a CTR, as shown in Fig. 2A. We adapted the magnetic gripper to a one DoF magnetic pivoting scalpel to show the applicability of our design. In addition, to increase the magnetic driving force, we presented a magnetic transmission mechanism to drive a

surgical forceps that can output Newton level gripping force and be used for resecting brain tissue. The end effector tools themselves were designed to be low cost and disposable. We conducted phantom experiments to evaluate the magnetic tools' workspace and output force, and in vivo experiments to evaluate their feasibility for clinical operations. These magnetic neurosurgical tools have the potential to pave the way for a new era of minimally invasive surgical tools designed for deep seated brain tumors, epilepsy, and other neurosurgical conditions.

The contributions of this work, building upon our previous research (*36-39*), are as follows: Firstly, we overview the design principles and actuation methods for magnetic surgical tools, while expanding the tool portfolio with the addition of a specialized magnetic cutter. Secondly, we define and integrate clinical requirements to develop an updated fully operational, clinically ready magnetic surgical tool system tailored to neurosurgical applications. Furthermore, we provide a first evaluation of the system's efficacy and safety through a comprehensive evaluation pipeline, incorporating phantom models and in vivo experiments.

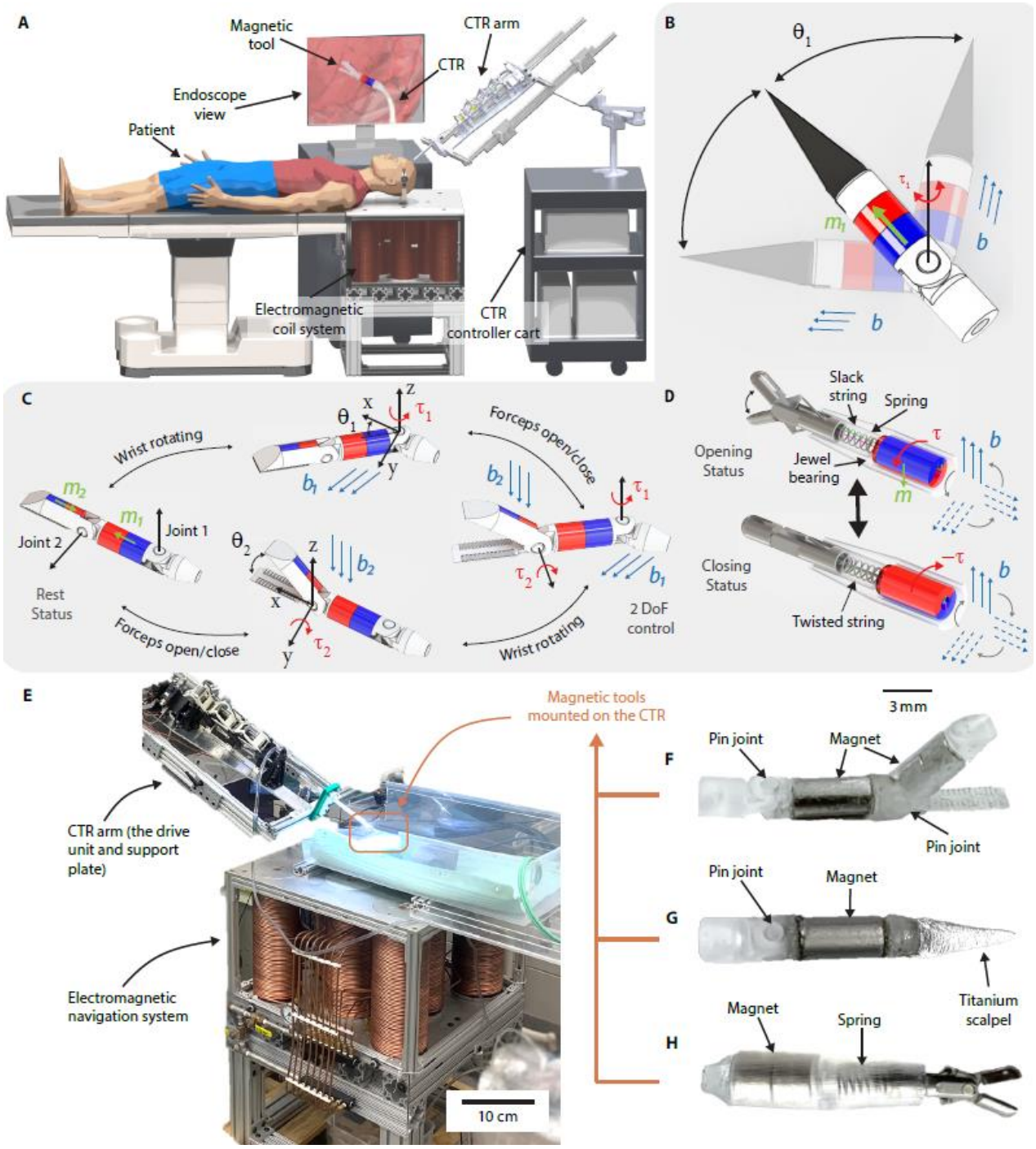

Figure 2. The proposed magnetic robotic system. **A.** Overview of the system that included magnetic tools, an electromagnetic navigation system, a concentric tube robot arm, and an endoscopy system. **B.** Illustration of the magnetic pivoting scissors design. **C.** Illustration of the magnetic wristed gripper design. **D.** Illustration of the magnetic TSA forceps design. **E.** The developed multi-component magnetic robotic system, and images of fabricated magnetic tools including **F.** the wristed gripper, **G.** the pivoting scalpel, and **H.** the TSA forceps.

RESULTS

Magnetic robot design

A magnetic wristed gripper was initially designed. As shown in Fig. 2C, the magnetic gripper consisted of two rotating joints connected in series: a wrist joint (Joint 1) and a jaw joint (Joint 2). Each moving link had a small cylindrical magnet attached to provide actuation torque. The revolution axes of the two joints were orthogonal to each other, which decoupled the gripper motions into two independent actuation DoFs and simplified robot control. To swing the gripper wrist, an external field $\mathbf{b}_1$ was created to induce a magnetic torque $\boldsymbol{\tau}_{b1}$ about Joint 1, aligning the wrist magnetization with the field $\mathbf{b}_1$, and rotating Joint 1 to the desired angle θ. The jaws of the gripper were normally closed as a consequence of the interaction of the magnets. As shown in Fig. s1, the magnetic torque $\boldsymbol{\tau}_{m2}$ and force $\boldsymbol{f}_{m2}$ induced by the jaw magnet $\mathbf{m}_2$ from the wrist magnet $\mathbf{m}_1$ dominated the jaw's movement over the gravity, keeping the jaws closed in the absence of an external actuation field. To open the jaws, a second external field $\mathbf{b}_2$ with its direction parallel to the revolution axis of Joint 1 (and perpendicular to the direction of the field $\mathbf{b}_1$) can be created to induce a magnetic torque $\boldsymbol{\tau}_{b2}$ on the jaw magnet, tilting the jaw. The gripper can be similarly closed by applying $\mathbf{b}_2$ in the opposite direction, or $\mathbf{b}_2$ can be reduced to zero to allow the inter-magnet force to close the jaws naturally.

The second magnetic end effector was a magnetic pivoting scalpel with 1 DoF swinging motion, as shown in Fig. 2B. The scalpel swing motion was induced in the same way as the wrist joint of the magnetic gripper. These two tools can be used for dexterous cutting and grasping in neurosurgery. In addition, the design can be tailored to other neurosurgical tools such as a cautery pen or a suction tube by replacing the end effector.

For cases such as tissue biopsy where a substantially larger force of hundreds of millinewtons was needed to cut or resect tissue, a third tool was used. The output force of the direct field actuation method used for the magnetic gripper and scalpel was restricted by the strength of magnetic field that can be reasonably generated, and may not be strong enough for the biopsy task. On this basis, we designed a magnetic twisted string actuator (TSA) forceps, as shown in Fig. 2D. Twisting strings can convert an input torque into a substantially magnified pulling force, and therefore provide sufficient force for tissue biopsy. The concept of the magnetic TSA transmission was introduced in our previous work (*39*) and in this paper, the TSA mechanism was scaled down to actuate a miniaturized biopsy forceps. In the design, a small cylindrical magnet was placed inside a 3D-printed shell and used to twist a double string. The string twisting induced a pull force which closed the forceps through a slider crank mechanism. A rotating actuation field $\mathbf{b}_t$ with its central axis collinear with the tool shaft was applied to rotate the magnet. A spring between the magnet and the forceps opened the forceps when the magnet was counter rotated.

Full magnetic robotic system implementation

We developed a multi-part magnetic robotic system aiming at performing neurosurgery in an operation room, as shown in Fig. 2E.

The three magnetic tools were fabricated (Fig. 2F-2H) with details described in Materials and Methods. The outer diameter of the tools were all less than 3.2 mm which ensured the

tools fit through the working channel of a neurosurgical trocar. The gripper jaw can open to angles up to 45° and the wrist/scalpel can each swing to angles up to ±60°. The overall length of the gripper from Joint 1 to the jaw tip was 20 mm (15 mm and 18 mm for the scalpel and the TSA forceps). The magnetic scalpel's swing accuracy and repeatability were experimentally measured (details in the Supplementary Material) under manual joystick control as 0.7 degrees and 0.3 degrees, respectively. Its swing workspace was measured as ±60 degrees. The tools were modular, and can be swapped by simply attaching the tools' connector to a holder by press fit. Off-the-shelf magnets were used in the end effectors to ensure a low cost.

Magnetic fields for actuation were generated by our custom electromagnetic navigation system (ENS) (*42*). The ENS consisted of eight water cooled electromagnets that were placed in a flat and parallel pattern. Such a table like layout provided a fully open workspace for the surgeon to access the patient and also for deploying assistive surgical devices (e.g., a robotic positioner, respiration hose, or irrigation pipe). It can generate a sustainable maximum field of up to 45 mT at its origin point which was 110 mm above the ENS's top surface center, a height that is typical of an adult human head. The ENS had a dimension of 60 cm×60 cm×85 cm and a weight of 450 kg, much more compact than many other ENS with comparable field strength and workspace (*43*, *44*).

A CTR was used as a steerable robotic positioner for the magnetic end effectors. The CTR was a miniature, flexible robotic system constructed from multiple concentric tubes that were both superelastic and precurved. These tubes were fabricated from a nickel titanium alloy, i.e., nitinol (NiTi), which can be pre-shaped to a desired curvature through a heat treatment process. After concentric assembly of the tubes, relative rotation and translation of each elastic tube resulted in a tentacle like motion with 6 DoFs (*45*, *46*). The reachable workspace of the CTR used here was evaluated in our previous work (*47*), and was in the shape of an inverted bell with diameter of 32 mm and height of 35 mm, which was large enough to cover most of the third ventricle of the human brain.

To ensure that the magnetic tools can generate sufficient output forces to manipulate brain tissue, a force sensor was employed to directly measure the pushing and jaw closing blocking forces under ENS actuation with a sustainable field value of 40 mT, as described in the Materials and Methods section. The force outputs of the magnetic scalpel and wrist, and the blocking force of the magnetic TSA forceps with continuous rotating turns and magnetic strength, were presented in Fig. s2. The measurement results shown in Table I were compared to the required forces in brain tissue operations (*40*), where the average forces on the major areas of the brain including the cerebrum, cerebellum, brainstem, and corpus callosum were considered. It can be seen that the magnetic wristed gripper was strong enough to push away brain tissue with its wrist and pick up the tissue with its gripper, and the magnetic TSA forceps can break the tissue and perform the biopsy task. For the articulated scalpel we measured the scalpel's pressing force, which was the same as the pushing force of the magnetic wristed gripper.

Table I Output forces of the magnetic tools under actuating field of 40 mT

Magnetic tools	Measured forces, mN (Mean value)	Averaged required forces, mN (*40*)	Capable operations
Gripper	Jaws closing: 98	Stab incision: 11	Picking up
Scalpel	Blade pressing: 181		Stab tissue

Gripper	Wrist pushing: 181	Carrying incision: 91	Pushing tissue
Scalpel	Blade pressing: 181		Cutting through
TSA forceps	Jaws closing: 350	Retraction: 98	Break and retract tissue

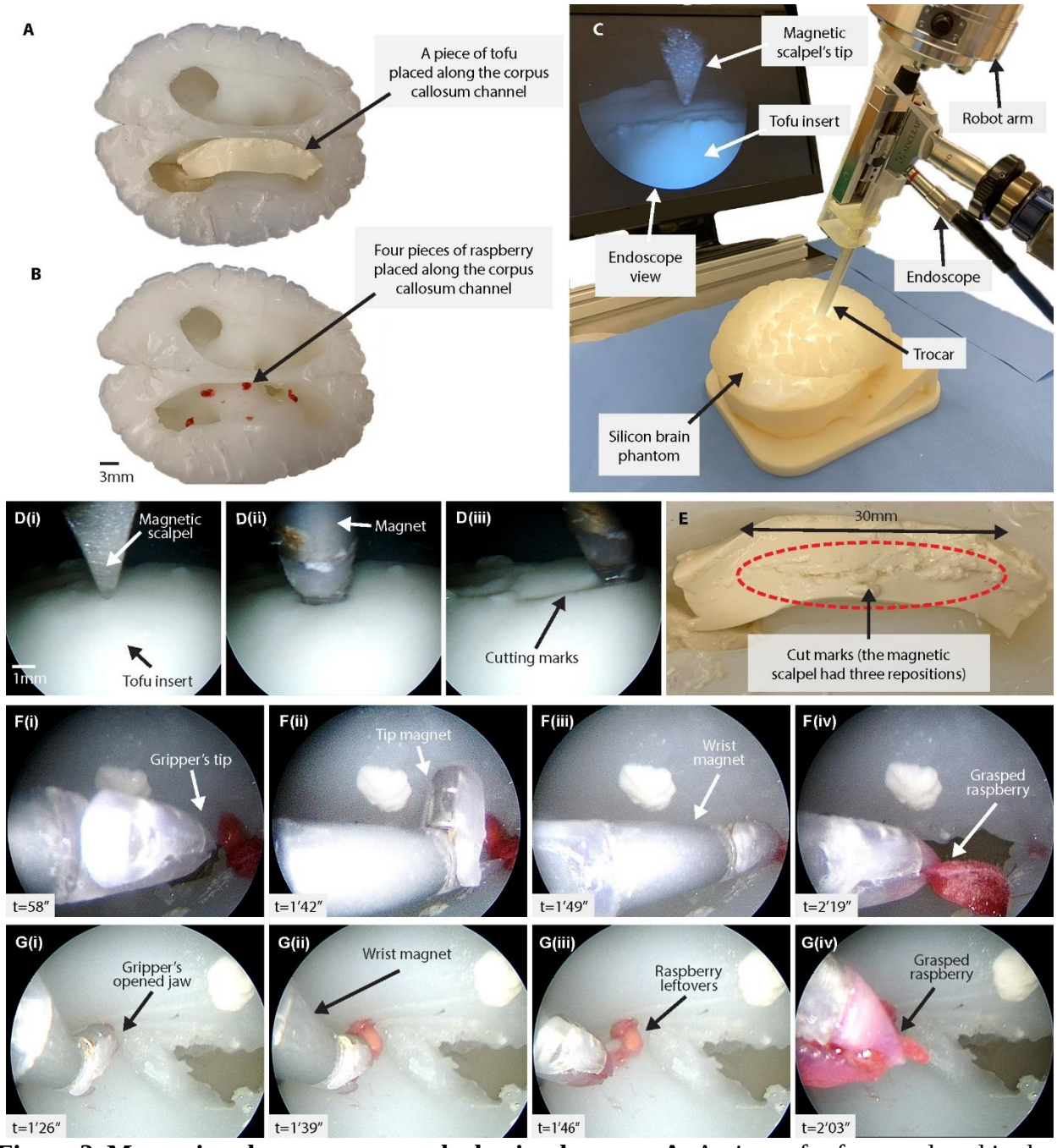

Figure 3. Magnetic robots operate on the brain phantom. **A.** A piece of tofu was placed in the brain phantom to mimic the corpus callosum. **B.** Four pieces of small raspberry were placed along the corpus callosum area to mimic the tumor tissue. **C.** The magnetic tool was positioned by a robot arm and inserted into the brain through the trocar's working channel with endoscopic visual feedback. **D(i)-D(iii).** The magnetic scalpel inserted into and cut the tofu by pivoting its blade. **E.** The tofu cut trace made by the magnetic scalpel. The magnetic wristed gripper picked up a piece of raspberry that was placed in the phantom's **F(i)-F(iv)** right side and **G(i)-G(iv)** left side.

Phantom experiments

A brain phantom was used to test the developed magnetic robotic system for its feasibility to conduct neurosurgical cutting tasks. The 3D printed brain phantom was modeled on anatomy (*48*), including important structures such as the third ventricle and corpus callosum channel. The silicone phantom was placed on a rigid 3D-printed skull which was fixed on the ENS top surface.

Two sets of experiments were conducted, including controlling the magnetic scalpel to perform simulated corpus callosotomy (cutting the corpus callosum fibers connecting the two hemispheres of the brain), and the magnetic wristed gripper for simulated tumor resection in the brain ventricle area. In the first experiment, a band of tofu was placed inside the phantom to mimic the corpus callosum, as shown in Fig. 3A, as its mechanical properties were roughly similar to that of brain tissue according to the advice of our experienced surgeon author JD. In the second experiment, three small pieces of raspberry were placed at three different locations inside the brain phantom along the corpus callosum channel, as shown in Fig. 3B, to mimic the tumor tissue. In both experiments, the magnetic tools were controlled wirelessly by the operator under the endoscope vision, as shown in Fig. 3C and Supplementary Videos s1 and s2. The experiments were repeated five times in both groups.

For the tofu cutting experiment, the tofu was taken out and visually observed to verify the cut "incision" with one example result shown in Fig. 3D and Fig 3E. The raspberry pick up tasks were exemplified in Fig. 3F and Fig. 3G, with the success rate calculated as 76% throughout the experiment where a successful pick up was counted only if the raspberry piece did not drop when the gripper retracted. The average time elapsed for a single pick up (from the gripper starting reaching the target to the gripper starting retracting) was recorded as 18 seconds.

We also conducted experiments to compare the tofu cutting performance between the magnetic scalpel and a standard surgical scalpel with procedures described in the Supplementary Methods. The standard scalpel produced uneven cuts, with groove widths of 2.1 mm, 0.7 mm, 0.8 mm, and 0.6 mm for the four users, whereas the magnetic scalpel achieved consistent and narrow paths, with an average width of 0.3–0.4 mm. Both manual and magnetic scalpels achieved substantial penetration, with average cutting depths of 2.6 mm, 3.4 mm, 7.1 mm, and 3.9 mm for the manual scalpel, compared to 4 mm for the magnetic scalpel.

In vivo experiments to demonstrate the feasibility of the tools in surgical procedures

The full magnetic robotic system in Fig. 2E was set up in a mock operating room at the Hospital for Sick Children for in vivo experiments to further evaluate the system's feasibility for neurosurgery operations in clinical environments. Three magnetic tools including the magnetic wristed gripper, magnetic scalpel, and magnetic TSA forceps were tested on two living piglets on two separate days, to allow for animal preparation and procedure review. The procedures were performed on the brain surface and brain ventricle area respectively. For both days' experiments, the piglets were placed under anesthesia beforehand, followed by a craniotomy to create a small burr hole in their skulls. The piglet was then moved to the ENS working table for robotic procedures, as shown in Fig. 4.

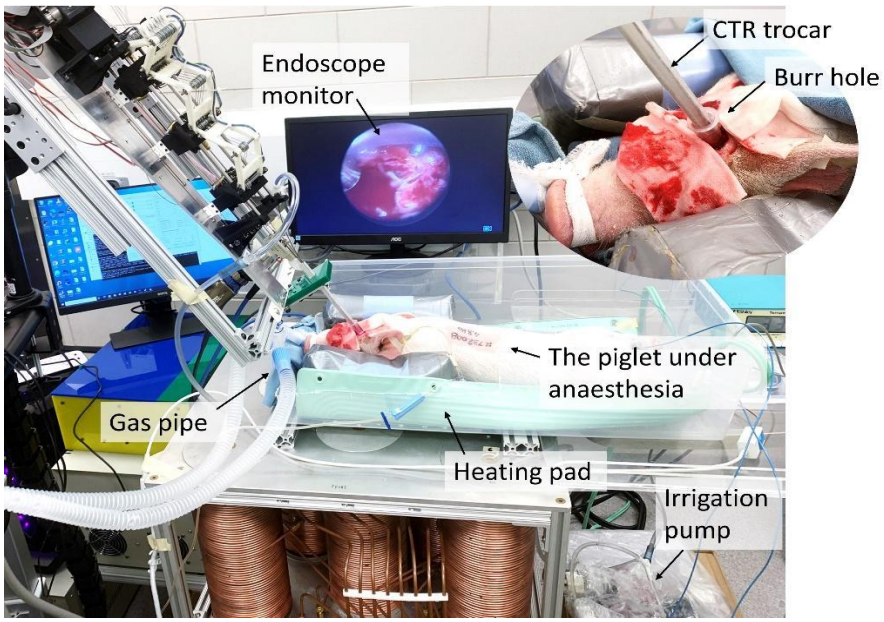

Figure 4. The operating room setup for the in vivo experiment. The anesthetized piglet was placed with its head right above the ENS system table center. A burr hole was created on the piglet's skull that provided the entry to insert the trocar into the brain.

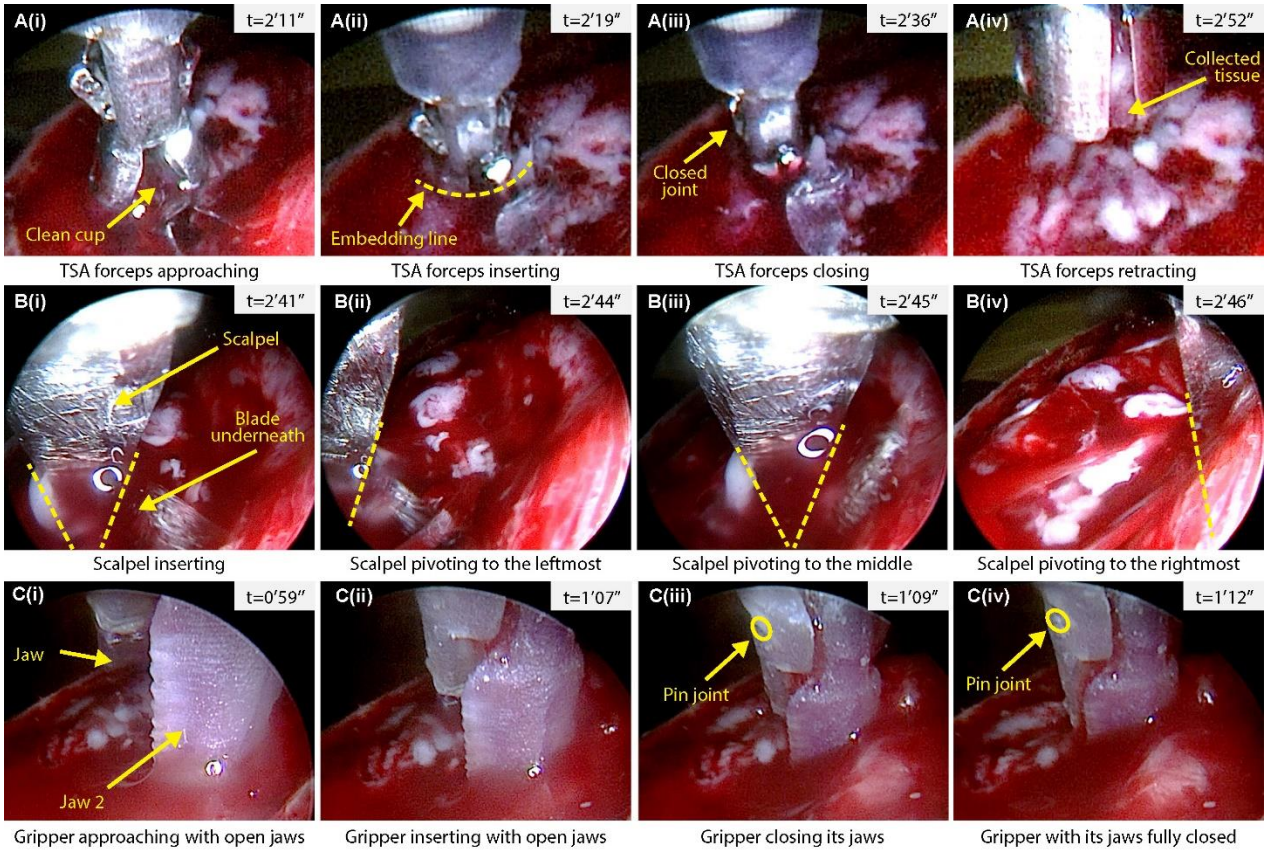

Figure 5. Magnetic robots operate on the surface of the piglet brain. A(i)-A(iv): The magnetic TAS forceps were controlled to resect the brain tissue; **B(i)-B(iv)**: the magnetic scalpel was controlled to cut through the brain tissue; **C(i)-C(iv)**: the magnetic gripper was controlled to perform a full closing motion with its jaws inserted into the brain tissue.

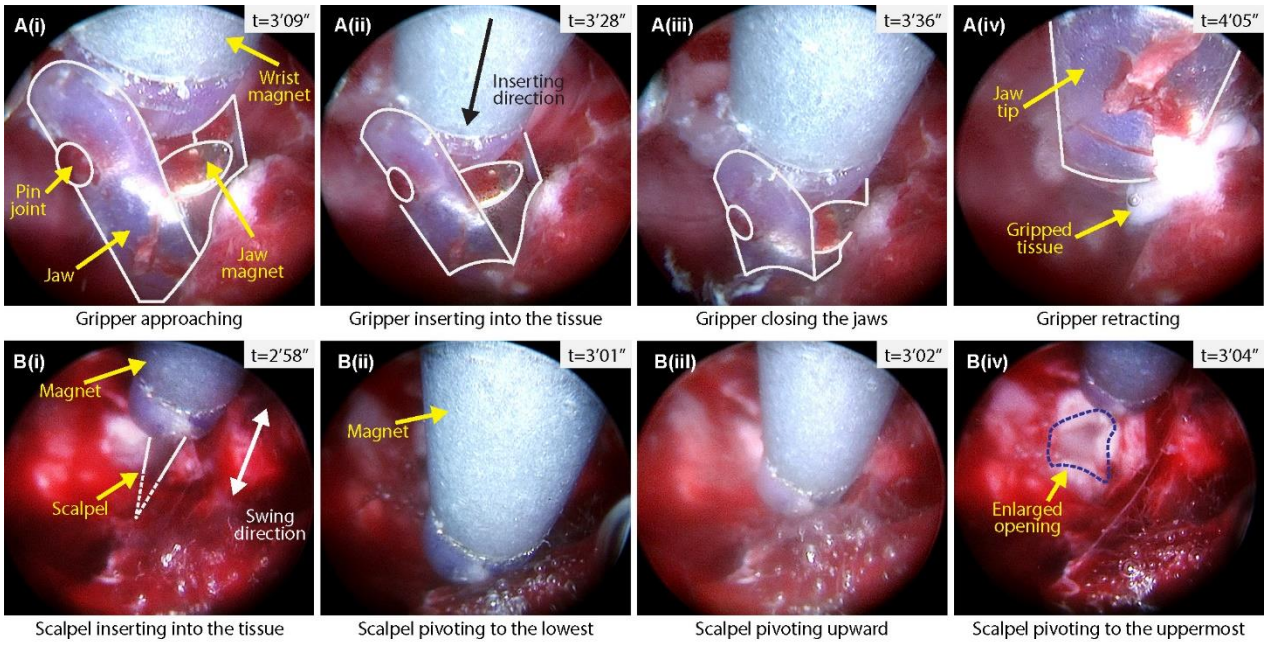

Figure 6. Magnetic robots operate in the ventricle of the piglet brain. A(i)-A(iv): The magnetic gripper was controlled to grip the tissue around the ventricle after its wrist was adjusted to the desired direction; **B(i)-B(iv)**: the magnetic scalpel was controlled to cut the tissue, creating an incision to access the ventricle.

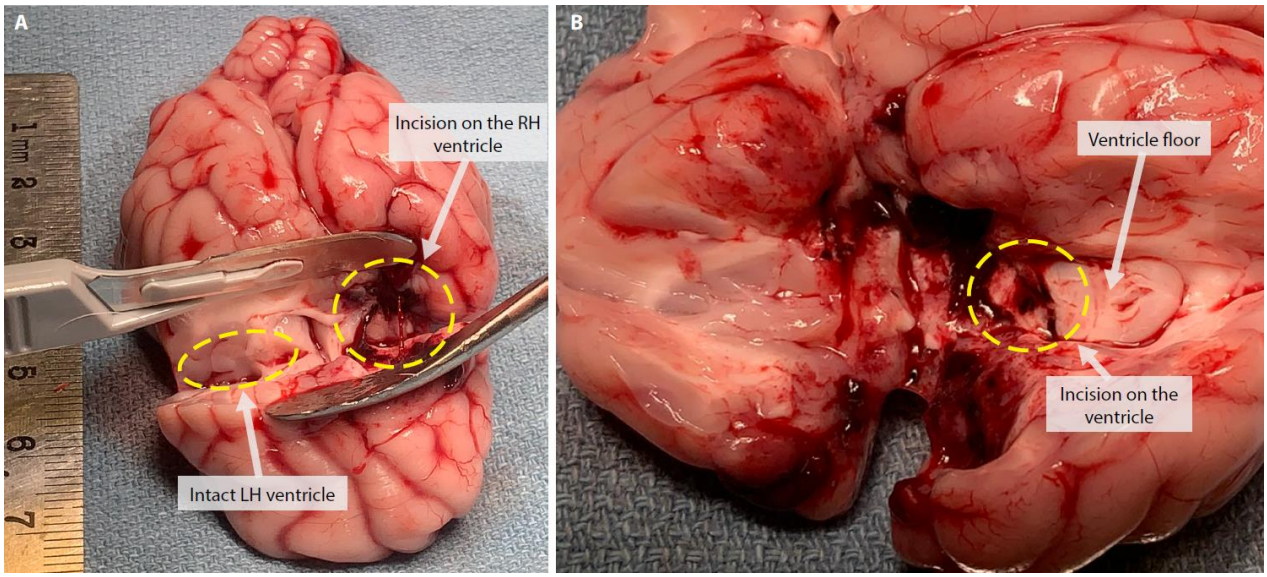

Figure 7. Necroscopy results for the ventricle incision. A. The ventricle of the right hemisphere (RH) had deep incisions. This demonstrated that the magnetic tools successfully reached the ventricle area and performed the mock procedures. In contrast, the ventricle areas of the left hemisphere (LH), which were not targeted, remained intact. **B.** The lateral cut section of the RH ventricle area showed the incision reached the ventricle depth and an opening was made to access the ventricle.

The day one experiment was performed with the goal of cutting through the brain surface tissue with the magnetic scalpel, pushing away the surrounding tissue with the magnetic gripper's wrist, and removing a piece of the surface tissue with the magnetic TSA forceps'

scoop jaws. Screenshots in Fig. 5 (taken from a video, see Supplementary Videos s3, s4, and s5) showed the procedure, through which it was seen that the scalpel could cut and tear the tissue with a full motion range, the gripper could successfully close its jaws in the bloody tissue environment while its tips were inserted in the tissue, and the TSA forceps could scoop the tissue with a full cup. A duration of 24 seconds was recorded for the tissue biopsy using the TSA forceps, 5 seconds for a cycle swing movement of the magnetic scalpel, and 13 seconds for the gripping operation using the magnetic wristed gripper. The TSA forceps required 5 seconds to fully close their jaws from the open position, a duration that could be further reduced to 0.1 seconds with a higher field operation frequency, as reported in our previous work (*49*).

On day two, we tested the magnetic tools to operate inside the deep brain area around the third ventricle. A corridor on the brain was made with a suction tube to allow the endoscope trocar to be inserted into the brain tissue and then facilitate the magnetic tools in reaching the third ventricle through the controlled delivery of the CTR. The magnetic scalpel was first controlled to cut an opening at the corpus callosum, then the magnetic gripper was used to grip a piece of tissue in the third ventricle. The procedures were recorded and shown in the Supplementary Videos s6 and s7, and Fig. 6. It can be observed that the scalpel could cut the tissue and make a visible opening around the ventricle, and the gripper could adjust its wrist to grasp the tissue in the deep brain with its tip pushing away the surrounding tissue. After the robotic tasks, a necroscopy was performed to inspect the incision made by the magnetic tools. As shown in Fig. 7, a substantial incision area appeared at the third ventricle of the left hemisphere, which indicated that the magnetic tools successfully performed the desired procedures in the designated area.

DISCUSSION

In this study, we introduced three magnetic tools: a magnetic 2-DoF gripper, a 1-DoF magnetic swing cutter, and a 1-DoF TSA forceps, along with a full magnetic robotic system for actuation, control, and positioning of the tools. The feasibility of these tools for clinical neurosurgical applications was demonstrated through successful gripping, cutting, and resection tasks performed on both tofu based phantoms and in vivo piglet models.

In the phantom experiments, the results showed that all pieces of tofu in the repeated five experiment sets were successfully cut by the magnetic scalpel, with visible stab incisions and cut traces along the entire length, suggesting the potential of the magnetic scalpel for real surgical operations. In the cutting comparison experiment, the magnetic scalpel produced substantially narrower incisions than the manual scalpel, indicating less potential damage to surrounding healthy tissue during an incision. The cutting width of the magnetic scalpel could be further reduced by incorporating a sharper and thinner blade. The cutting depth of the magnetic scalpel is adjustable by controlling the advancement of its positioner. In this experiment, it was set to approximately 4 mm, showcasing the tool's capability to achieve sufficient penetration while maintaining precision. In the simulated tumor resection experiment, the failure cases were mainly caused by the lack of stereovision feedback with a standard neuroendoscope, which caused insufficient grasping depth of the raspberry pieces. The success rate can be improved if a stereo-endoscope was used to provide the operator with depth perception. Nevertheless, the magnetic wristed gripper showed great potential for performing pick up tasks in neurosurgery.

In the surface tissue operation of the living piglet brain experiments, the dura mater contributed to the observed mixed cutting and tearing action due to its toughness and resilience. This limitation underscores the need for improved sharpening techniques for the magnetic scalpel to enhance its cutting efficacy. In practical endoscopic procedures, where the dura mater is bypassed, the scalpel is expected to perform more effectively.

A piglet brain, although it has similar tissue, is much smaller than a human brain, and does not provide large enough space for our human scale tool to operate. Thus the in vivo experiments did not include all realistic surgical procedures, such as cutting the corpus callosum along its length and grasping tissue inside the third ventricle. Nevertheless, we showed that the magnetic tools can perform certain fundamental movements and operations, which indicates the potential for translation to human subjects. The live piglets were used over cadaver piglets, as cadaver heads showed degenerated brain tissue (ventricle was collapsed and the blood was clotted resulting in limited available operation space and unclear endoscopic vision inside the brain) and thus do not provide adequate operation space and clear endoscopic vision for the magnetic tools.

The diameter of the robotic end effectors presented was 3.18 mm. Smaller diameter tools may be even more capable of advanced dexterity in the cramped space available in the brain, but the actuation force of the magnetic tools becomes unreasonably low at smaller sizes considering the ENS power limit. A larger field could be created by a more powerful ENS, but with tradeoffs in size, weight, and heat generation.

This work adopted a human-in-loop manual control strategy for the operator to command the magnetic tools, with the priority of evaluating the tools' feasibility for tissue operation. Such intuitive control is adequate for the demonstrations shown but this setup will make it straightforward to add computer assistance and implement automation control. Future work will investigate this by integrating feedback systems such as flexible pressure (*50*) and imaging sensors (*51*) and incorporating advanced control frameworks (52, 53). Our previous work has shown the positioning accuracy and step response of the magnetic tools under the stereovision based closed loop control are sufficiently good (*41*), indicating the magnetic tools are promising for dynamic control. Nonetheless, this study does not specifically evaluate the efficacy of the adopted human-in-the-loop control strategy, representing a potential limitation of the complete system, which will be addressed in future works by a user study.

Our cableless magnetic end effector design can offer versatility in surgical applications. It can be fabricated with a hollow channel running through its length, providing a free working channel for accommodating additional functions such as irrigation or suction (*47*). This feature enhances the tool's multifunctionality while maintaining a compact and minimally invasive design.

When placed into an endoscope channel, the magnetic wristed tool could occlude the endoscopic view when the tool bends toward the endoscope lens. This could be mitigated by using a flexible endoscope (*54*).

The material of the CTR tubes is NiTi which has negligible magnetic responsiveness. The magnetic forces and torques acting on the tools are approximately 0.1 N and do not impact the CTR's mechanics due to the high stiffness of the NiTi tubes.

Our magnetic robotic system meets all the requirements from operation force, device size, to modulation, and open operating workspace around the patient. Currently, the magnetic tools are partly assembled with 3D printed parts, which can be sterilized if biocompatible resin material is used. Compared to a standard endoscopic tool whose workspace is limited by the trocar as a short straight line, our magnetic tools provide an enlarged motion range at the tooltips with adequate motion accuracy.

MATERIALS AND METHODS

Magnetic tool fabrication

The magnetic tools were fabricated with off-the-shelf small permanent magnets and 3D-printed resin parts. All the small magnets were purchased from SuperMagnetMan online shop. The 3D printings were conducted with a FormLabs Form3 printer with ClearV4 resin material. For the magnetic wristed gripper, a cylinder magnet Cyl0126 was used for the wrist joint link and two stacked cylinder magnets Cyl0053 were used for the jaw joint link. The magnets and the 3D printed joints were attached with Loctite® super glue 416. The same magnet was used for the magnetic scalpel for its wrist joint. For the magnetic TSA forceps, two stacked tube magnets (Tube0115D) were used as the rotor which was installed to a jewel ring bearing. Two strands of cotton strings were used to connect the rotary tube magnets and the biopsy forceps' push wires with the super glue. A steel compression spring was installed around the cotton strings and used to restore the biopsy forceps to open status.

Magnetic tool actuation

When an external magnetic field is applied to a magnetic material, the latter is subjected to a magnetic torque and tends to align its magnetization direction with the field direction. The magnetic torque $\boldsymbol{\tau}_{bi} \in R^3$ can be calculated as a vector cross product between the magnetic moment $\boldsymbol{m}_i \in R^3$ of the magnetic material and the field $\boldsymbol{b} \in \mathbf{R}^3$ where the magnetic material is considered as a dipole at its mass center:

$$\boldsymbol{\tau}_{bi} = \boldsymbol{m}_i \times \boldsymbol{b} = \begin{bmatrix} 0 & -m_{iz} & m_{iy} \\ m_{iz} & 0 & -m_{ix} \\ -m_{iy} & m_{ix} & 0 \end{bmatrix} \boldsymbol{b}. \quad (1)$$

Besides the magnetic torque $\boldsymbol{\tau}_{bi}$ generated from an external field, the magnetic material $\boldsymbol{m}_i$ also receives an interference force $\boldsymbol{f}_{mi} \in \mathbf{R}^3$ from the adjacent magnetic volume $\boldsymbol{m}_j$.

$$\boldsymbol{f}_{mi} = \frac{3\mu_0}{4\pi\|\boldsymbol{r}_{ji}\|^4}\left(\left(\hat{\boldsymbol{r}}_{ji}^{\mathsf{T}}\boldsymbol{m}_i\right)\boldsymbol{m}_j + \left(\hat{\boldsymbol{r}}_{ji}^{\mathsf{T}}\boldsymbol{m}_j\right)\boldsymbol{m}_i + \left(\boldsymbol{m}_j^{\mathsf{T}}\boldsymbol{m}_i - 5\left(\hat{\boldsymbol{r}}_{ji}^{\mathsf{T}}\boldsymbol{m}_j\right)\left(\hat{\boldsymbol{r}}_{ji}^{\mathsf{T}}\boldsymbol{m}_i\right)\right)\hat{\boldsymbol{r}}_{ji}\right), \quad (2)$$

where $\boldsymbol{r}_{ji}$ is the distance vector between $\boldsymbol{m}_i$ and $\boldsymbol{m}_j$, and $\hat{\boldsymbol{r}}_{ji} = \boldsymbol{r}_{ji}/\|\boldsymbol{r}_{ji}\|$. $\mu_0 = 4\pi\times10^{-7}$ $\mathrm{T\cdot m\cdot A^{-1}}$ is the permeability of free space.

With these formulations, we can develop actuation models for the magnetic tools (*55*). For the magnetic wristed gripper, as shown in Fig. 2C, the wrist rotary actuating torque $\boldsymbol{\tau}_1$ can be obtained directly from (1) and the jaw opening actuating torque $\boldsymbol{\tau}_2$ was a subtraction of the magnetic torque and the interference torque as $\boldsymbol{\tau}_2 = \boldsymbol{\tau}_{b2} - \boldsymbol{f}_{m2} \times \boldsymbol{d}_2 - \boldsymbol{\tau}_{m12}$, where $\boldsymbol{d}_2$

was the distance vector between the joint 2 and jaw magnet $\boldsymbol{m}_2$ and $\boldsymbol{\tau}_{m12}$ was the inter-magnet torque that magnet $\boldsymbol{m}_2$ applied to magnet $\boldsymbol{m}_1$. Then the equation of motion for the gripper can be written as $\boldsymbol{H\ddot{\theta}} = \boldsymbol{\tau}_C(\dot{\boldsymbol{\theta}}, \boldsymbol{\theta}) + \boldsymbol{\tau}_K(\boldsymbol{\theta}) + \boldsymbol{\tau}_a$ (*56*), where $\boldsymbol{\theta} = [\theta_1, \theta_2]$ was the magnetic robot' joint vector, H was the inertia matrix, $\boldsymbol{\tau}_C$ and $\boldsymbol{\tau}_K$ were Coriolis and gravity force components, $\boldsymbol{\tau}_a = [\boldsymbol{\tau}_1, \boldsymbol{\tau}_2]$ was the actuating torque.

The same actuation model of the magnetic gripper can be applied to the magnetic scalpel's wrist rotary actuating torque $\boldsymbol{\tau}_1$. For the magnetic TSA forceps, the rotary actuating torque can be obtained from (1) and the motion equation can be resolved similar to the gripper. In these models we assumed the frictions in the pin joints were considered as negligible.

Generating magnetic field

The field was generated and controlled by modulating the input currents of the ENS. The ENS had eight coils and each of them individually created a magnetic field (*42*). Magnetic fields superimpose linearly in air, which allows the magnetic field at any given position to be determined as a vector summation of all the individual fields, as shown by a simulation result in Fig. s3. The correlation between the input currents and the generating field can be obtained either by simulation or by experimentation (*57*, *58*) where the latter was chosen in this work. A calibration matrix was calculated for the field at the ENS origin point and used to modulate the input currents (*42*), which was described as $[\boldsymbol{b}, \boldsymbol{G}] = C \cdot \boldsymbol{i}$, where $\boldsymbol{G} = \left[\frac{\partial b_x}{\partial x} \ \frac{\partial b_x}{\partial y} \ \frac{\partial b_x}{\partial z} \ \frac{\partial b_y}{\partial y} \ \frac{\partial b_y}{\partial z}\right]$ was the five independent field gradients and not used in this work, $C \in \mathbf{R}^{8\times8}$ was the calibration matrix, and $\boldsymbol{i} \in \mathbf{R}^8$ was the current vector.

Concentric tube robot

The CTR's tip pose $\boldsymbol{u}=[p_x, p_y, p_z, \alpha, \beta, \gamma]^T$ can be adjusted by changing its three pre-curved tubes' extended lengths (l_1, l_2, l_3) and orientations (φ_1, φ_2, φ_3). The method in (*45*) was used to calculate the inverse kinematics of the CTR with the input of $\boldsymbol{u}$ to resolve the desired tube configurations $\boldsymbol{x}$, where $\boldsymbol{x} = [l_1, l_2, l_3, \varphi_1, \varphi_2, \varphi_3]^T$.

Magnetic tool output force measurement

The magnetic tools were mounted at their customized jigs and placed at the origin position of the ENS as shown in Fig. s4. A load cell (LSB200, FUTEK, USA) was used as the force sensor to directly measure the tools' output forces. The ENS was controlled to generate fields of up to a moderate magnitude of 40 mT to actuate the tools. While our ENS could generate larger fields up to 85 mT, it couldnot sustain such high fields for more than a few minutes which was not practical for tool characterization.

Phantom experimental setup

The setup for the phantom experiment was shown in Fig. 3C. For the tofu cutting task, the magnetic scalpel was mounted to a slender NiTi tube with its installation hole and press fit approach, while the NiTi tube itself was mounted on a collaborative robot arm (Franka Robotics, Germany). In the experiment, the magnetic scalpel was manually positioned in the brain phantom through an endoscopic trocar. The scalpel wrist joint was then actuated for cutting by the magnetic field under operator's joystick control. When a target area of the tofu was fully cut, the trocar was then manually re-oriented to adjust the scalpel's

cutting range to cover the tofu's entire surface. For the simulated brain tumor resection task, the magnetic scalpel was simply replaced by the magnetic wristed gripper at the NiTi tube's tip thanks to their modular design. In the experiment, an operator manipulated the gripper remotely via a joystick with endoscopic camera feedback to reach and pick up the raspberry piece.

In vivo experimental setup

In the in vivo experiment, the CTR was used to hold and provide steerable positioning for the magnetic tools. An operator controlled the CTR arm and the magnetic tools using a joystick with visual feedback from an endoscope. Two Yorkshire female piglet animals were used: one 6 weeks old and with 5.5 kg weight and the other 5 weeks old and with 4.8 kg weight. The piglets were anesthetized with inhaled anesthetics throughout the experiments and placed on a heating pad to keep the body warm. The animals were euthanized after the experiments. An animal use protocol (AUP 63103) with the experiment procedures was reviewed and approved by the Animal Care Committee of the Hospital for Sick Children.

Robotic system control strategy

We adopted a human-in-the-loop control strategy for the magnetic robotic system, as illustrated in Fig. s5. The operator's commands to the robotic system were conveyed by a joystick and transmitted to the CTR and the ENS using a proportional mapping approach. The magnetic tool was then actuated by the field generated by the ENS and positioned by the CTR based on the operator's inputs. The endoscope image was used as the feedback to close the control loop which allowed the operator to dynamically compensate for the magnetic tool's motion errors. In the experiments, the phantoms and animal models' positions on the ENS were preplanned to locate the magnetic tool's workspace around the ENS origin point (11 cm above the center of the ENS top surface), to facilitate actuating the magnetic tools by modulating the field at ENS's origin.

References

1. K. T Thakur, E. Albanese, P. Giannakopoulos, N. Jette, M. Linde, M. J Prince, T. J Steiner, T. Dua, in *Disease Control Priorities*, V. Patel, D. Chisholm, T. Dua, R. Laxminarayan, and M. E. Medina-Mora, Eds. (Int. Bank for Recon. and Dev./The World Bank, Washington, DC, 2016), vol. 4, chap. 5.
2. P. Kwan, M. J. Brodie, Early identification of refractory epilepsy. *N. Engl. J. Med*. **342**, 314-9 (2000).
3. Y. Schiller, Y. Najjar, Quantifying the response to antiepileptic drugs: effect of past treatment history. *Neurology*. **70**, 54-65 (2008).
4. L.M. Auer, P. Holzer, P.W. Ascher, F. Heppner, Endoscopic neurosurgery. *Acta Neurochir.* **90**, 1–14 (1988).
5. D. T. Oberlin, A. S. Flum, J. D. Lai, J. J. Meeks, The effect of minimally invasive prostatectomy on practice patterns of American urologists. *Urol. Oncol. Semin. Orig. Investig.* **34**, 255-e1 (2016).
6. M. Innocentim, G. Malzone, G. Menichini, First-in-human free flap tissue reconstruction using a dedicated microsurgical robotic platform. *Plast. Reconst. Surg*. 151, 1078-1082 (2023).
7. Sony Group Corporation, Sony group portal website, May 9, 2024, https://www.sony.com/en/SonyInfo/News/Press/202405/24-020E/ (2024)
8. P. Karl, J. Peine, M. Mencattelli, Y. Chitalia, D. Pu, T. Looi, S. Stone, J. Drake, P. E. Dupont, Using robotics to move a neurosurgeon's hands to the tip of their endoscope. *Sci. Robot.* **8**, eadg6042 (2023).
9. V. Bodani, H. Azimian, T. Looi, J. Drake, Design and evaluation of a concentric tube robot for minimally-invasive endoscopic paediatric neurosurgery, i*n Proceedings of Hamlyn Symposium on Medical Robotics* (2014), 12 to 15 July 2014, London, pp. 25-26.
10. B. Jessica, D. C. Rucker, H. B. Gilbert, P. J. Swaney, P. T. Russell, K. D. Weaver, R. J. Webster, A telerobotic system for transnasal surgery. *IEEE/ASME Trans. on Mechatronics*. **19**, 996-1006 (2013).

11. T. Anor, J.R. Madsen, P. Dupont, Algorithms for design of continuum robots using the concentric tubes approach: A neurosurgical example, i*n Proceedings of the 2011 IEEE International Conference on Robotics and Automation*, 9 to 13 May 2011, Shanghai, China, pp. 667-673.
12. M.F. Rox, D. S. Ropella, R. J. Hendrick, E.Blum, R. P. Naftel, H. C. Bow, S. D. Herrell, K. D. Weaver, L. B. Chambless, R. J. Webster III, Mechatronic design of a two-arm concentric tube robot system for rigid neuroendoscopy. *IEEE/ASME Trans. on Mechatronics*. **25**, 1432-1443 (2020).
13. Y. Kim, S. S. Cheng, J. P. Desai, Active Stiffness Tuning of a Spring-Based Continuum Robot for MRI-Guided Neurosurgery. *IEEE Trans. on Robotics.* **34**, 18-28 (2018).
14. S. S. Cheng, X. Wang, S. Jeong, M. Kole, S. Roys and R. P. Gullapalli, Mechanical Design and Evaluation of a Selectively-actuated MRI-compatible Continuum Neurosurgical Robot, *in Proceedings of the 2021 IEEE/RSJ International Conference on Intelligent Robots and Systems*, 27 September to 01 October 2021, Prague, Czech Republic, pp. 2498-2503.
15. T. Veiga, J. Chandler, P. Lloyd, G. Pittiglio, N. Wilkinson, A. Hoshiar, R. Harris, P. Valdastri, Challenges of continuum robots in clinical context: a review. *Prog. Biomed. Eng*. **2**, 032003 (2020).
16. M. Sitti, H. Ceylan, W. Hu, J. Giltinan, M. Turan, S. Yim, E. Diller, Biomedical applications of untethered mobile milli/microrobots. *Proc. IEEE*. 103, 205-224 (2015).
17. B. Han, Z. C. Ma, Y. L. Zhang, L. Zhu, H. Fan, B. Bai, Q. D. Chen, G. Z. Yang, H. B. Sun, Reprogrammable soft robot actuation by synergistic magnetic and light fields. *Adv. Funct. Mater*. 32, 2110997 (2022).
18. M.J. Lang, A.D. Greer, G.R. Sutherland, in *Intraoperative Imaging*, M. Pamir, V. Seifert, T. Kiris, Eds. (Springer, Vienna, 2011), vol 109, pp 231–236.
19. D. von Langsdorff, P. Paquis, D. Fontaine, In vivo measurement of the frame-based application accuracy of the Neuromate neurosurgical robot. *J. Neurosurg.* **122**, 191-194 (2015).
20. J. González-Martínez, B. Juan, T. Susan, G. John, S. Saksith, N. Imad, B. William, Technique, results, and complications related to robot-assisted stereoelectroencephalography. *Neurosurgery.* **78**, 169-180 (2016).
21. M. Sitti, H. Ceylan, W. Hu, J. Giltinan, M. Turan, S. Yim, E. Diller, Biomedical applications of untethered mobile milli/microrobots. *Proc. IEEE*. **103**, 205-224 (2015).
22. B. J. Nelson, S. Pané, Delivering drugs with microrobots. *Science.* **382**, 1120-1122 (2023)
23. Y. Sehyuk, M. Sitti, Design and rolling locomotion of a magnetically actuated soft capsule endoscope. *IEEE Trans. on Robotics*, **28**,183-194 (2011).
24. S. Zheng, J. Nan, M.C. Hoang, M. Nan, K.T. Nguyen, J. Kim, J. Park, G. Go, E. Choi, Magneto-responsive polymeric soft-shell-based capsule endoscopy for high-performance gastrointestinal exploration via morphological shape control. *Adv. Intell. Syst*. **6**, 2300632 (2024).
25. Y. Sehyuk, E. Gultepe, D. H. Gracias, M. Sitti, Biopsy using a magnetic capsule endoscope carrying, releasing, and retrieving untethered microgrippers. *IEEE Trans. Biomed. Eng*. **61,** 513-521 (2013).
26. Z. Li, Y. P. Lai, E. Diller, 3D printing of multilayer magnetic miniature soft robots with programmable magnetization. *Adv. Intell. Syst.* **6**, 2300052 (2024).
27. H. Li, G. Go, S.Y. Ko, J.O. Park, S. Park, Magnetic actuated pH-responsive hydrogel-based soft micro-robot for targeted drug delivery. *Smart Materials and Structures*, **25**, 027001 (2016).
28. Y. P. Lai, Z. Li, H. Naguib, E. Diller, Hybrid Hydrogel-Magnet Actuators with pH-Responsive Hydrogels for Gastrointestinal Microrobots. *Adv. Eng. Mater*. **25**, 2301060 (2023).
29. P. Shokrollahi, Y.P. Lai, S. Rash-Ahmadi, V. Stewart, M. Mohammadigheisar, L.A. Huber, N. Matsuura, A.E. Zavodni, J. Parkinson, E. Diller, Blindly controlled magnetically actuated capsule for noninvasive sampling of the gastrointestinal microbiome. *IEEE/ASME Trans. on Mechatronics*. **26**, 2616-2628 (2020).
30. X. Wang, Z. Gong, T. Wang, J. Law, X. Chen, S. Wanggou, J. Wang, B. Ying, M. Francisco, W. Dong, Y. Xiong, J. Fan, G. Macleod, S. Angers, X. Li, P. Dirks, X. Liu, Y. Sun, Mechanical nanosurgery of chemoresistant glioblastoma using magnetically controlled carbon nanotubes. *Sci. Adv.* **9**, eade5321 (2023).
31. Y. Kim, E. Genevriere, P. Harker, J. Choe, M. Balicki, R. W. Regenhardt, J. E. Vranic, A. A. Dmytriw, A. B. Patel, X. Zhao, Telerobotic neurovascular interventions with magnetic manipulation. *Sci. Robotics*. **7**, eabg9907 (2022).
32. C. Chautems, A. Tonazzini, Q. Boehler, S. H. Jeong, D. Floreano, B. J. Nelson, Magnetic continuum device with variable stiffness for minimally invasive surgery. *Adv. Intell. Syst*. **2**, 1900086 (2020).
33. G. Pittiglio, P. Lloyd, T. da Veiga, O. Onaizah, C. Pompili, J. H. Chandler, P. Valdastri, Patient-specific magnetic catheters for atraumatic autonomous endoscopy. *Soft Robotics.* **9**, 1120-1133 (2022).
34. C.M., Heunis, K. J. Behrendt, E. EG Hekman, C. Moers, JP. PM de Vries, S. Misra, Design and evaluation of a magnetic rotablation catheter for arterial stenosis. *IEEE/ASME Trans. on Mechatronics*. **27**, 1761-1772 (2021).
35. Z. Yang, L. Yang, M. Zhang, Q. Wang, SCH. Yu, L. Zhang, Magnetic control of a steerable guidewire under ultrasound guidance using mobile electromagnets. *IEEE Robot. Autom. Lett*. **6**, 1280-1287 (2021).
36. C. Forbrigger, A. Lim, O. Onaizah, S. Salmanipour, T. Looi, J. Drake, and E. Diller, Cable-less, magnetically-driven forceps for minimally invasive surgery. *IEEE Robot. Autom. Lett*. **4**, 1202–1207 (2019).
37. A. Lim, A. Schonewille, C. Forbrigger, T. Looi, J. Drake and E. Diller, Design and comparison of magnetically-actuated dexterous forceps instruments for neuroendoscopy. *IEEE Trans. on Biomed. Eng.* **68**, 846-856 (2021).
38. O. Onaizah, E. Diller, Tetherless mobile micro-surgical scissors using magnetic actuation, in *Proceedings of the 2019 IEEE International Conference on Robotics and Automation*, 20 to 24 May 2019, Montreal, QC, pp. 894-899.

39. M. Nica, C. Forbrigger, E. Diller, A novel magnetic transmission for powerful miniature surgical robots. *IEEE/ASME Trans. on Mechatronics*. **27**, 5541-5550 (2022).
40. H. J. Marcus, K. Zareinia, L. S. Gan, F. W. Yang, S. Lama, G.-Z. Yang, G. R. Sutherland, Forces exerted during microneurosurgery: a cadaver study. *Int. J. Med. Robot. Comput. Assist. Surg*. **10**, 251–256 (2014).
41. C. Forbrigger, E. Friden, E. Diller, Evaluating the feasibility of magnetic tools for the minimum dynamic requirements of microneurosurgery, in *Proceedings of the 2023 IEEE International Conference on Robotics and Automation*, 29 May to 2 June 2023, London, pp. 4703-4709.
42. A. Schonewille, C. He, C. Forbrigger, N. Wu, J. Drake, T. Looi, E. Diller, Electromagnets under the table: an unobtrusive magnetic navigation system for microsurgery. *IEEE Trans. Med. Robot. Bionics*. **6**, 980-991 (2024).
43. M. P. Kummer, J. Abbott, B. E. Kratochvil, R. Borer, A. Sengul, B. J. Nelson, OctoMag: an electromagnetic system for 5-DOF wireless micromanipulation. *IEEE Trans. on Robotics*. **26**, 1006-1017 (2010).
44. J. Sikorski, I. Dawson, A. Denasi, E. E. G. Hekman, S. Misra, Introducing BigMag — A novel system for 3D magnetic actuation of flexible surgical manipulators, in *Proceedings of the 2017 IEEE International Conference on Robotics and Automation*, 29 May to 3 June 2017, Singapore, pp. 3594-3599.
45. P. E. Dupont, J. Lock, B. Itkowitz, E. Butler, Design and control of concentric-tube robots. *IEEE Trans. on Robotics.* **26**, 209-225 (2009).
46. R. J. Webster, J. M. Romano, N. J. Cowan, Mechanics of precurved-tube continuum robots. *IEEE Trans. on Robotics*. **25**, 67-78 (2009).
47. C. He, R. Nguyen, C. Forbrigger, J. Drake, T. Looi, E. Diller, A hybrid steerable robot with magnetic wrist for minimally invasive epilepsy surgery, in *Proceedings of the 2023 IEEE International Conference on Robotics and Automation*, 29 May to 2 June 2023, London, pp. 6830-6836.
48. G. E. Breimer, V. Bodani, T. Looi, J. M. Drake, Design and evaluation of a new synthetic brain simulator for endoscopic third ventriculostomy, *J. Neurosurg. Pediatr*. **15**, 82–88, (2015).
49. H. Mayer, J. Drake, E. Diller, T. Looi, Compact Magnetic Twisted String Actuated Forceps for Stronger Robot-Assisted Neuroendoscopy, in *Proceedings of the 2024 Hamlyn Symposium on Medical Robotics*, 25 to 28 June 2024, London, pp 65-66.
50. A. Aubeeluck, C. Forbrigger, S. M. Taromsari, T. Chen, E. Diller, H. E. Naguib, Screen-printed resistive tactile sensor for monitoring tissue interaction forces on a surgical magnetic microgripper. *ACS Appl. Mater. Interfaces.* **15**, 34008–34022 (2023).
51. X. Liu, D. Esser, B. Wagstaff, A. Zavodni, N.Matsuura, J. Kelly, E. Diller. Capsule robot pose and mechanism state detection in ultrasound using attention-based hierarchical deep learning. *Sci. Rep.* **12**, 21130 (2022).
52. J. Li, D. Li, C. Wang, W. Guo, Z. Wang, Z. Zhang, H. Liu. Active collision avoidance for teleoperated multi-segment continuum robots toward minimally invasive surgery. *Int. J. Robot. Res*. **43**, 918-41 (2024).
53. T. Yang, Y. Yang, P. Wang, Y. Cao, Z. Yang, H. Liu. A lumen-adapted navigation scheme with spatial awareness from monocular vision for autonomous robotic endoscopy. *Robot. Auton. Syst*. **165**, 104444 (2023).
54. J. Kim, T. Looi, A. Newman and J. Drake, Development of deployable bending wrist for minimally invasive laparoscopic endoscope, in *Proceedings of the 2020 IEEE/RSJ International Conference on Intelligent Robots and Systems*, 25 to 29 October 2020, Las Vegas, pp. 3048-3054.
55. J. Abbott, E. Diller, A. Petruska, Magnetic methods in robotics. *Annual Review of Control, Robotics, and Autonomous Systems*. **3,** 57-90 (2020).
56. R. Featherstone, D. E. Orin, in *Springer Handbook of Robotics*, B. Siciliano and O. Khatib, Eds. (Springer, Berlin, 2016), pp. 35–65.
57. S. L. Charreyron, Q. Boehler, B. Kim, C. Weibel, C. Chautems, B. J. Nelson, Modeling electromagnetic navigation systems. *IEEE Trans. on Robotics*. **37**, 1009-1021 (2021).
58. A. J. Petruska, J. Edelmann, B. J. Nelson, Model-based calibration for magnetic manipulation. *IEEE Trans. Magn.* **53**, 1-6 (2017).
59. C. A. Schneider, W. S. Rasband, K. W. Eliceiri, NIH Image to ImageJ: 25 years of image analysis. *Nature Methods*, **9**, 671–675 (2012).

Acknowledgments: The authors thank Marvin Estrada and Anson Lam for preparing the animals for the in vivo experiments. The authors thank Adam Waspe for performing MRI scans for the experimental animals.

Funding: Canadian Institutes of Health Research Grant 452287 (ED, JD)

Author contributions:

Conceptualization: CH, TL, JD, ED
Methodology: CH, RN, HM, LC, ED
Investigation: CH, RN, HM, PK, AA, GT, TL, EF
Visualization: CH, LC, HM, PK
Supervision: TL, JD, ED

Funding acquisition: TL, JD, ED
Writing – original draft: CH and LC
Writing – review & editing: CH, LC, RN, JD, TL, ED

Competing interests: Authors declare that they have no competing interests.

Data and materials availability: All data are available in the main text or the supplementary materials.

Supplementary Methods

Motion performance evaluation of the magnetic joint

We quantitatively evaluated the magnetic joint's motion accuracy under the human-in-the-loop control approach using the magnetic scalpel. As shown in Fig. s6(a), the tool was fixed at its anterior end above a paper protractor placed on the ENS table. A 12 MP camera (ArduCam, IMX477) was mounted directly above to record the experiment. The user controlled the scalpel remotely with a joystick to move its tip to specific protractor scales, ranging from 90 to 150 degrees at 10-degree intervals. The joint center of the scalpel was aligned with the protractor's origin to facilitate alignment. Screenshots were taken from the video stream when the scalpel paused at each scale, and ImageJ (*59*) was used to measure the angle between the scalpel and the target scale, as illustrated in Fig. s6(b). The experiment was repeated eight times to minimize manual measurement deviations. The mean absolute error of the pivoting angle was calculated to assess motion accuracy, and the standard deviation represented motion repeatability. To measure the workspace, the scalpel was actuated to its extreme swing positions, and the corresponding protractor scale readings were recorded to determine the pivoting range. A supplementary video of an example operation is included as Supplementary Video s8.

Comparison of tofu cutting using manual and magnetically actuated tools

The magnetic scalpel was mounted on a linear stage, with its tip aimed at a block of tofu placed on the ENS surface. The tofu was marked with 12 pairs of blue dots, and the scalpel was sequentially moved over each pair, swinging to cut through the tofu. The scalpel's insertion depth was manually adjusted via the linear stage to ensure the tip was embedded. After cutting, red dye was applied to highlight the paths, and the tofu was resected along the common midline of each column to visualize cutting depth, as shown in Fig. s7. For comparison, a standard surgical scalpel was manually operated on new tofu samples by four users: the engineer author RN, the senior author TL, a non-author engineer, and a non-author craniofacial surgeon. The users practiced several times before the experiment to ensure consistency. Both cutting width w and depth d were measured using a caliper.

Supplementary Figures

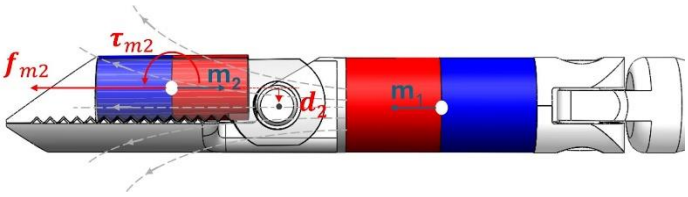

Figure S1. Static force analysis for the gripper. The gray dashed lines represent the magnetic field generated by the wrist magnet $\mathbf{m}_1$. The arrow represents the field direction. $\boldsymbol{\tau}_{m2}$ and $\boldsymbol{f}_{m2}$ are the magnetic torque and force received by the jaw magnet $\mathbf{m}_2$ from the wrist magnet $\mathbf{m}_1$ which stabilizes the jaws at the closed configuration.

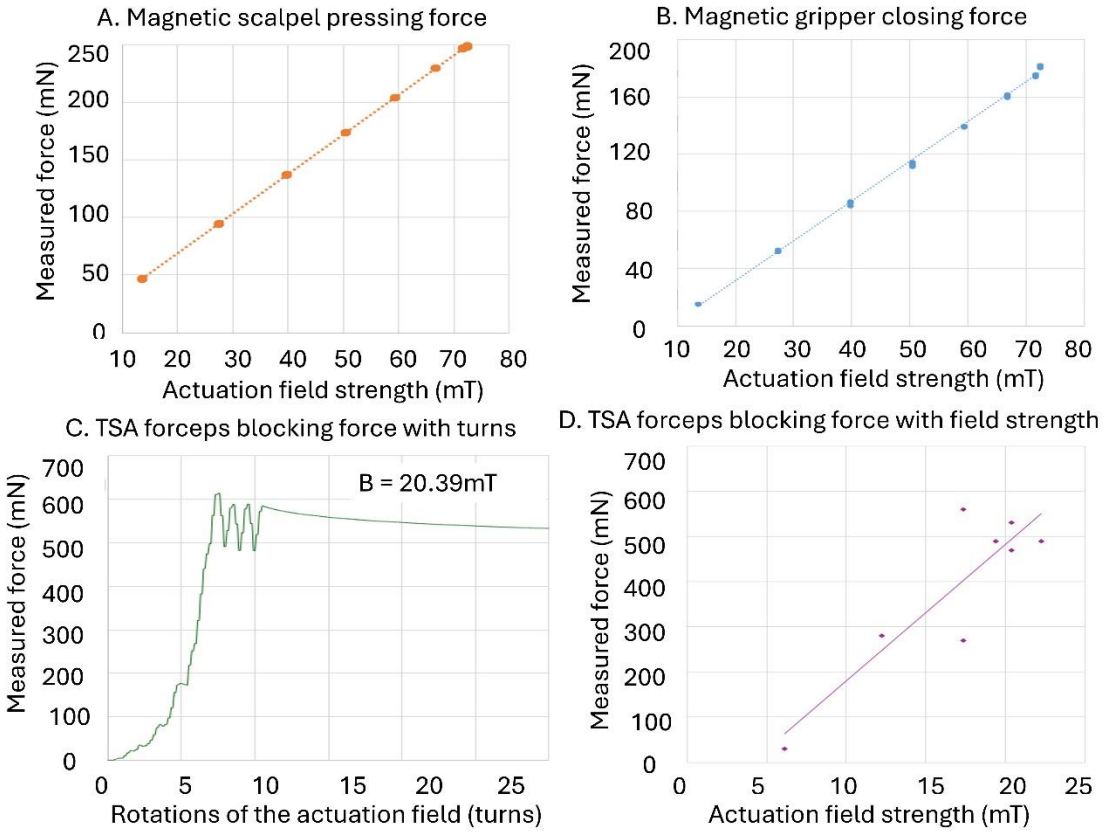

Figure S2. Force output of the magnetic tools. A. The magnetic scalpel blocking force as a function of the field strength; B. The magnetic gripper closing force as a function of the field strength; C. The magnetic TSA forceps blocking force (jaws closing force) as a function of the rotating turns of the actuation field of 20 mT. The TSA blocking force saturates after 6-8 turns. D. The magnetic TSA forceps blocking force as a function of the field strength. Increasing the applied magnetic field can generate a larger blocking force because the bigger input magnetic torque can overcome the string resisting torque.

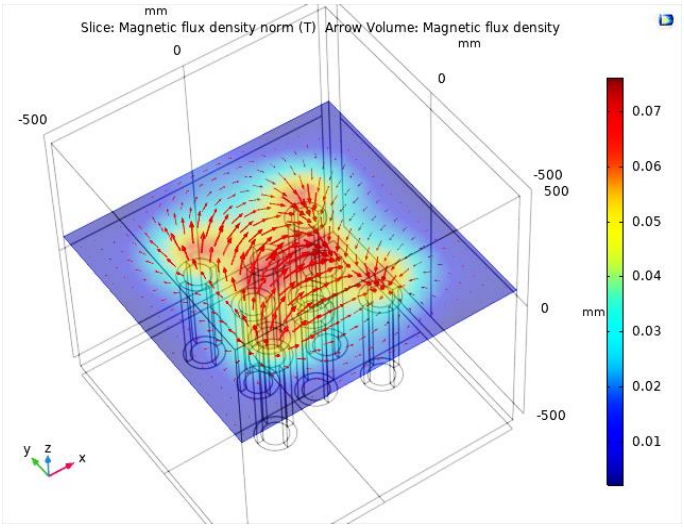

Figure S3. An example magnetic flux density of the ENS. The field is created at the surgical site in the *x*-direction.

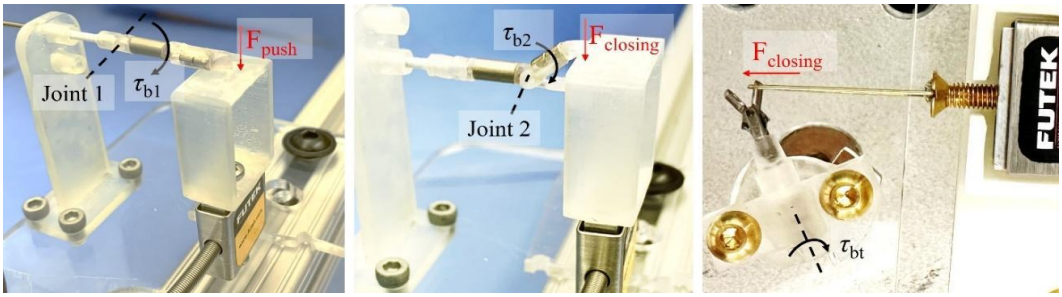

Figure S4. Force measurement setup for the magnetic gripper's wrist blocking force in the pushing direction (left), the magnetic gripper's jaw's closing force (middle), and the magnetic TSA forceps closing force (right).

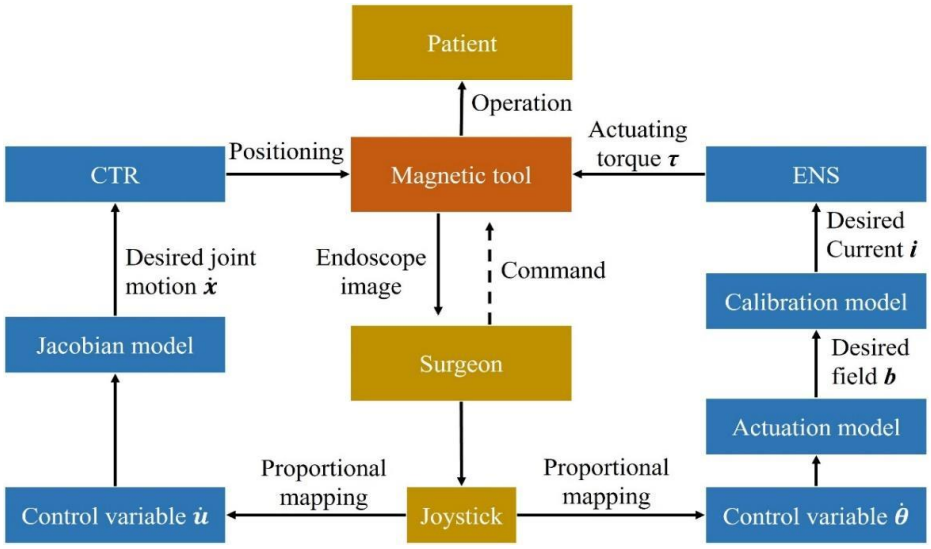

Figure S5. The human-in-the-loop control strategy used in controlling the robotic system.

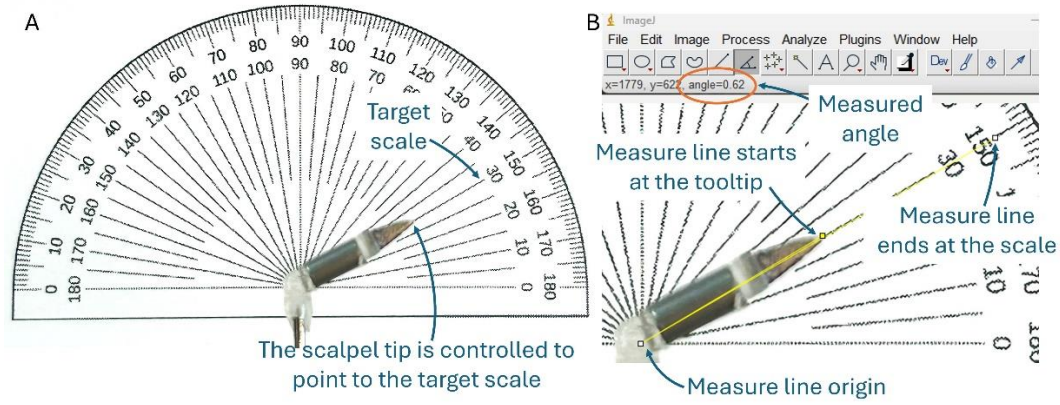

Figure S6. A. **Experimental setup for the magnetic scalpel's motion accuracy measurement** as observed by a camera. B. Zoom-in picture showing the angle measurement between the scalpel and the target scale.

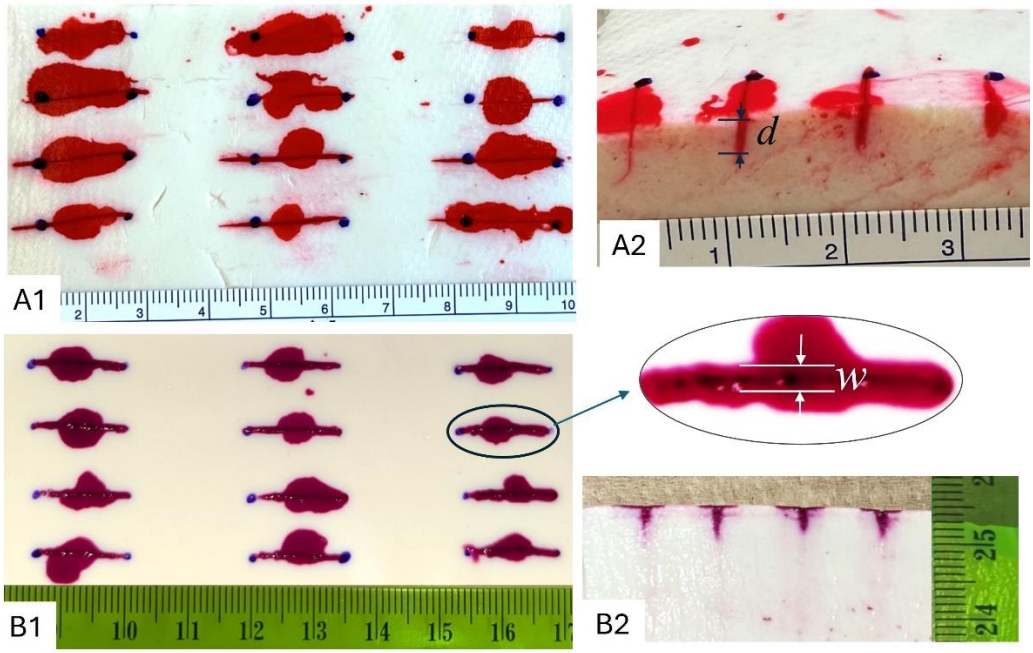

Figure S7. Comparative experiment for tofu cutting performance. A1 and A2: Top view and one of the section views of the tofu cut by the magnetic scalpel. B1 and B2: Top view and one of the section views of the tofu cut by a non-author surgeon with a standard scalpel manually. Red dye is added after the slicing as a visual contrast. The unit of the scales is mm.

Supplementary Videos

s1. Magnetic scalpel cut tofu in the phantom experiment.

s2. Magnetic wristed gripper picked up raspberry in the phantom experiment.

s3. Magnetic TSA forceps biopsied surface tissue in the in vivo experiment.

s4. Magnetic wristed gripper gripped surface tissue in the in vivo experiment.

s5. Magnetic scalpel cut surface tissue in the in vivo experiment.

s6. Magnetic scalpel cut ventricle tissue in the in vivo experiment.

s7. Magnetic gripper gripped ventricle tissue in the in vivo experiment.

s8. Magnetic scalpel motion accuracy test.